Vidal *et al. Geothermal Energy* 2023, **11**(1):18
https://doi.org/10.1186/s40517-023-00260-8

Geothermal Energy

RESEARCH Open Access

Structural control of the graben fault on hydrothermal alteration in the Cerro Pabellón geothermal system (Andean Cordillera, Northern Chile)

J. Vidal[1*], P. Patrier[2], D. Beaufort[2], S. Maza[1], G. Rivera[3], G. Volpi[3] and D. Morata[1]

*Correspondence:
jeannevidal@ing.uchile.cl

[1] Department of Geology and Andean Geothermal Center of Excellence (CEGA), Faculty of Physical and Mathematical Sciences, University of Chile, Plaza Ercilla 803, Santiago, Chile
[2] University of Poitiers, CNRS UMR7285, IC2MP, HydrASA, Bat B8, Rue Albert Turpain, TSA51106, F-86073 Poitiers Cedex 9, France
[3] ENEL Green Power Chile and Andean Countries. Av., Santa Rosa 76, Santiago, Chile

Abstract

This study focuses on hydrothermal alteration in the geothermal reservoir of Cerro Pabellón (Andean Cordillera, Northern Chile). It is based on CP2A and CP5A production wells drilled above a local normal fault and presenting unlike hydraulic properties. Cuttings from 300 to 1555 m depth were sampled and analyzed using X-ray diffraction (XRD) to observe distribution of hydrothermal minerals and crystal chemistry variations of clays (fraction < 5 µm). Then, scanning electron microscopy coupled with energy dispersive spectroscopy (SEM–EDX) allowed to perform microanalysis of hydrothermal minerals. These results highlight a mineral assemblage that was not observed before, composed of adularia + Ba-rich feldspar + feathery quartz + chalcedony + calcium arsenates + illite. They are characteristics of high-temperature hydrothermal alteration in epithermal settings and are restricted to shallow permeable fracture zones of the active part of the reservoir. Another fracture-controlled event related to a typical illitization is observed in all permeable fracture and fault zones of the geothermal system. This multi-event alteration seems strongly controlled by the eastern graben fault and the associated interconnected fracture network.

Keywords: Geothermal reservoir, High-enthalpy system, Low-sulfidation epithermal system, Clay minerals, Hydrothermal alteration, Cerro Pabellón, Chile, Andean Cordillera

Introduction

Hundreds of inferred and assessed geothermal areas in strong spatial and genetic relationships with the Quaternary volcanism and regional tectonic structures were identified along the Andean Cordillera (Aravena et al. 2016; Morata et al. 2021; Veloso et al. 2019). Main geothermal systems occur in the Central Andean Volcanic Zone (CAVZ) (14–28°S) where several geothermal exploration and exploitation projects were developed in the Chilean side. The most advanced exploration programs have been carried out at Colpitas, Surire, Puchuldiza, Pampa Lirima, Irruputuncu–Olca, and El Tatio-La Torta where geochemical, geological, and geophysical surveys were conducted (Aguirre et al. 2011; Aravena et al. 2016; Arcos et al. 2011; Cumming et al. 2002; Reyes

et al. 2011). MT campaigns, gas and water discharges surveys, and sometimes drilling of exploratory wells allow to assess the occurrences of geothermal resources (Legault et al. 2012; Tassi et al. 2010; Vidal et al. 2021). Although the Andean Cordillera represents one of the most attractive geothermal developments in the world, it remains also one of the largest undeveloped. The reason of the poor geothermal activity and development in Chile is mainly due to regulatory, political, and economic barriers and not the absence of geothermal resources. The recent citizen campaign *Chao Carbon* striving for a complete decarbonization by 2030 and recent policies for energy generation pointing to a 100% renewable matrix by 2050 give a new opportunity for the geothermal development in Chile (Morata et al. 2021). Geothermal energy is one of the best compromises in terms of low CO_2 emissions among the renewable energy sources. However, the increase of geothermal energy leans on minimizing the economic risks and thus, a better understanding of geothermal resources.

A better understanding of geothermal resources relies on direct access to the deep reservoir that remains limited with only few wells that intersect circulating hot fluids. Thirteen wells were drilled in the Cerro Pabellón (CP) geothermal field, located at 4500 m a.s.l, ~ 100 km northeast of Calama city (Antofagasta region, Northern Chile), near the Chile-Bolivia border. Since 2017, Geotérmica del Norte (GDN), a joint venture between Enel Green Power Chile and ENAP (Chilean National Oil Company) has exploited the unique commercial geothermal plant in South America with a power capacity of 81 MWe (two binary units of 24 MWe each one and additional 33 MWe expanded during 2022) (Cappetti et al. 2021).

This unique access to deep geothermal reservoir has been documented from a petrographic and mineralogical study of cuttings from CP wells (Maza et al. 2018; Vidal et al. 2022). Vidal et al. (2022) concluded that fractured zones that channel the ascending hot fluid were associated with a strong illitization superimposed over trioctahedral clay minerals from a previous propylitic alteration. Such a clay signature observed inside and outside of the Pabelloncito graben structure suggests a similar source for hydrothermal fluids which circulate in the fracture network related to border graben faults. As clay minerals are very sensitive to temperature, F/R ratio, time, nature of hydrothermal fluids, and fluid state among other factors, they are qualitative indicators to understand the geodynamics of deep circulations (Flexser 1991; Inoue and Kitagawa 1994; Patrier et al. 1996; Vásquez et al. 2016).

However, up today there is no published work focused on structural control of the graben border faults which exert a major structural control on deep fluids upwelling. The present paper is based on cuttings samples from CP5A and CP2A wells, both intersecting the graben border fault but presenting different productivity index. A mineralogical characterization of hydrothermal alteration with petrographic observations, X-Ray diffraction, and chemistry analysis was done in order to identify the geodynamics of deep circulations. The alteration signature will be compared to previous results from CP4A and CP6A wells. These original results aim to discuss the influence of graben faults on present-day productivity of the reservoir. They will help to better understand the hydrothermal flow in a deep Andean reservoir and strengthen the confidence for future geothermal developers in Chile.

The Cerro Pabellón geothermal system

Within the regional compressional regime related to the subduction of the Nazca Plate under the South American Plate, several local extensional features is observed with a Pliocene-extensional phase. Discovered in 1999 (previously referred as the 'Apacheta geothermal project' by Urzúa et al. 2002), the CP geothermal system is located inside a graben structure called the Pabelloncito graben associated to a NW-striking normal fault system (Fig. 1b). The NW tectonic trend is commonly observed in the CAVZ acting as structural weakness for hydrothermal and magmatic manifestations (Giordano et al. 2013; Godoy et al. 2014; Tibaldi et al. 2009; Veloso et al. 2019). The geology of the area has been widely described by Rivera et al. (2021).

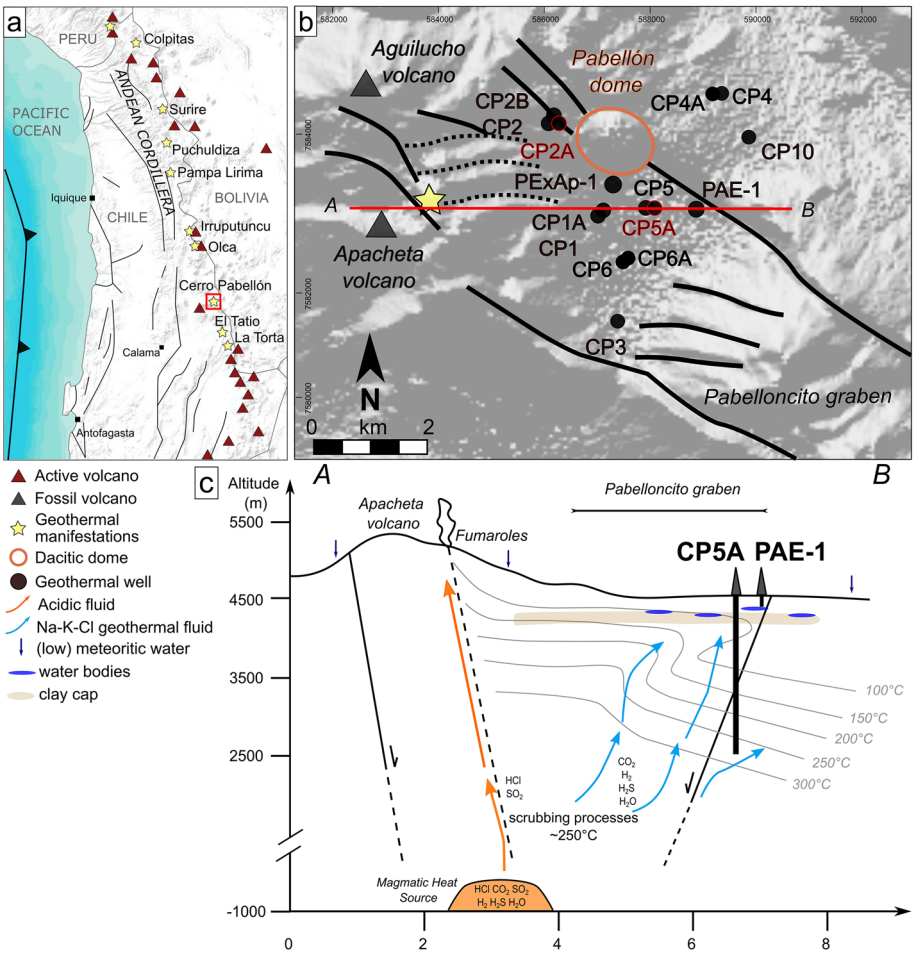

Fig. 1 **a** Map of the Central Andean Volcanic Zone (CAVZ), regional scale faults, active volcanoes, and main geothermal manifestations (geysers, fumaroles, steam grounds, hot springs, etc.) in the Chilean side after Aravena et al. (2016). The image used in the background is from ESRI. The red square is the studied area, also detailed in (**b**) Map of Cerro Pabellón (CP) geothermal wells with main normal faults and morphological lineaments (dashed line). CP5A and CP2A wells, in red, present samples analyzed in this study. The trace AB through the production well, CP5A, and the shallow water well, PAE-1, is presented in (**c**) Schematic profile with isotherms data after Urzúa et al. (2002), simplified geology, and traces of the intersected fracture and fault zones (FZs) are from Rivera et al. (2021) and Baccarin et al. (2021). Conceptual model of fluids is from Giudetti and Tempesti (2021); Taussi et al. (2019); Urzúa et al. (2002); and Vidal et al. 2022)

Exploration and deep wells drilled at CP are unique witnesses of the geothermal reservoir and confirmed occurrences of permeable fault and fracture zones (FZs) acting as preferential pathways for geothermal fluid (Baccarin et al. 2021; Vidal et al. 2022). The study of hydrothermal alteration in CP4A and CP6A wells evidenced a great spatial and temporal heterogeneity of alteration within in the deep reservoir (Vidal et al. 2022). At least two different styles of alteration were identified: (1) A weak to moderate pervasive alteration style which is characterized by little obliteration of the original textures and by replacement of most of the original rock-forming minerals by trioctahedral clays (saponite, corrensite, chlorite–corrensite mixed layers (C-Crr), and Fe–Mg chlorite), calc silicates (epidote, titanite, zeolites), and less frequently clays from celadonite-glauconite group. (2) A fracture-controlled alteration style which is characterized by a strong destruction of the original textures and in which both original rock-forming minerals and minerals from pervasive alteration have been dissolved and replaced by illite + illite–smectite mixed layers (I-S) + Fe- chlorite + carbonates (mainly calcite). As an active system, dynamic of fluids leads to an heterogeneous alteration; the dioctahedral sequence is mainly expressed in CP6A well, in the *hot core* inside the graben, whereas the trioctahedral sequence is mainly expressed in CP4A well, outside the graben. However, illitic minerals and more particularly I/S R3 ml (ill > 90%) are observed as clay signature for FZs in both wells inside and outside the graben suggesting a unique source for fluids circulating in the reservoir (Fig. 1c).

Secondary minerals from the two aforementioned alteration events were encountered in core samples from reservoir part of PexAP-1 exploration well, in addition to adularia, pyrite, and chalcopyrite (Maza et al. 2018). In this exploration well, a thick clay cap was also identified with variable amounts of smectite (montmorillonite–beidellite), R0 to R3 I-S, chlorite–smectite mixed layers, corrensite, and C-Crr. This thick clay cap guarantees the sealing of the reservoir preventing surficial hydrothermal manifestations inside the graben structure (Maza et al. 2018; Taussi et al. 2019). However, superheated fumaroles displaying high temperatures in a range of 108–119 °C, and a fossil alteration zone with pervasive hydrothermal alteration was observed at ~ 5,000–5,200 m a.s.l. on the top of the Apacheta-Aguilucho Volcanic Complex at the NW of the graben (Tassi et al. 2010; Urzúa et al. 2002) (Fig. 1b). Others warm springs with temperature around 23 °C were observed around 17 km SW of the power plant location (Urzúa et al. 2002). These fumarolic activities are associated with acidic sulfate to argillic alteration with kaolinite, opal CT, alunite, smectite, I-S, and illite (Maza et al. 2021a, 2021b).

The fluid circulating in the CP reservoir is a typical Na–K-Cl geothermal fluid with high solutes content and low gas content (Giudetti and Tempesti 2021). However, the fluid sampling occurs in surface and fluid probably suffered degassing that led to an increase of solutes compared to the deep reservoir. Regarding gases, CO_2 is the dominant species, whereas H_2 and CH_4 are strongly depleted. The recalculated pH at reservoir conditions is between 5 and 6.2. Na–K geothermometer indicates apparent equilibrium temperatures in the range of 280–290 °C, higher than the 255 °C measured in the hotter wells suggesting that the system could be even hotter at depth. The actual geochemical conceptual model-based δD- $\delta^{18}O$ isotopes and ^{14}C and ^{3}H ages suggest infiltration of meteoric waters that migrate from the recharge zone to the geothermal reservoir interacting with volcanogenic host rocks at high temperatures (> 250 °C) and

mixed with a possible magmatic water (Fig. 1c) (Giudetti and Tempesti 2021; Morata et al. 2019). Scrubbing processes of the ascending fluids could occur within the deep reservoir as suggested by typical magmatic gases, i.e., SO_2 and HCl, detected in superheated fumaroles in the Apacheta-Aguilucho Volcanic Complex and not detected in the geothermal fluid (Tassi et al. 2010). However, the relations in time and space between the geothermal fluid and the acidic fluids observed in the fumaroles are still uncertain and require further geochemical studies.

Shallow discontinuous water bodies were identified during drilling operations by GDN correlating MT survey below the Pabelloncito graben (Fig. 1c) (Urzúa et al. 2002). Water wells in the area reported high temperature and bubble gas. In the eastern margin of the graben, a shallow water well named PAE-1 (Fig. 1) produces a wispy flow of steam with a measured temperature of 88 °C, around the boiling point at 4500 m a.s.l. The condensate sample from this well highly depleted in $\delta^{18}O$ suggests multiple boiling and condensation processes at shallow depths (Urzua et al. 2002).

Wells of the study

The 3D thermal model of the CP reservoir shows a dome shape of the isotherms (Fig. 1c) (Baccarin et al. 2021). The apex of the thermal dome marks the center of the upflow zone of the geothermal fluid in the NW edge of Pabelloncito graben. Production wells from platforms CP-1, CP-5, and CP-6, drilled in the hot core of the reservoir, present great productivity. However, the productivity of CP-5 platform results from shallower permeable levels (400–700 m depth) compared to other wells of the hot core (1200–2200 m depth). Moreover, permeable FZs have been identified in andesitic lavas, while they are mainly located in tuffs in other wells (Baccarin et al. 2021). Production wells from CP-2 platform located at the northern limit of the thermal dome. The present study focuses on two production wells drilled between 2015 and 2017 during development stage intersecting the major graben fault: CP5A well drilled at the apex of the reservoir upflow zone, and CP2A well drilled in the northern margin of the upflow zone.

The well CP5A was drilled vertically until 1936 m depth above the eastern border fault of the graben. The temperature was acquired only until 600 m where it reaches 220 °C (Fig. 2). A permeable FZ was identified at 447 m depth, in andesitic lavas, with total mud losses during drilling and a negative temperature (T) anomaly in the T profile. However, the injectivity index of this FZ is low (Rivera et al. 2018). Partial mud losses were also observed at 525 m depth even if the structural model of Baccarin et al (2021) does not identify permeable FZ at this depth. A permeable FZ at 700 m depth is identified as the main structure responsible of the major injectivity (circa 7 m^3/h/bar) (Rivera et al. 2018). Total mud losses occurred at 1000 m depth making collect of cuttings impossible below this depth. The graben border fault was intersected at this depth according to the structural model of Rivera et al. (2021). Production test of the well revealed a total fluid flow rate of 305 t/h with a title of vapor of 18% (Rivera et al. 2018).

On the northern margin of the thermal dome, temperature decreases gradually below the CP-2 platform. Wells from CP-2 platform were drilled where the eastern border fault divides in three strands. The CP2A well was drilled vertically above the median strand of the fault until 2500 m depth (Fig. 1b). The temperature acquired ten months after drilling operations reaches circa 245 °C at 1800 m depth (Fig. 3).

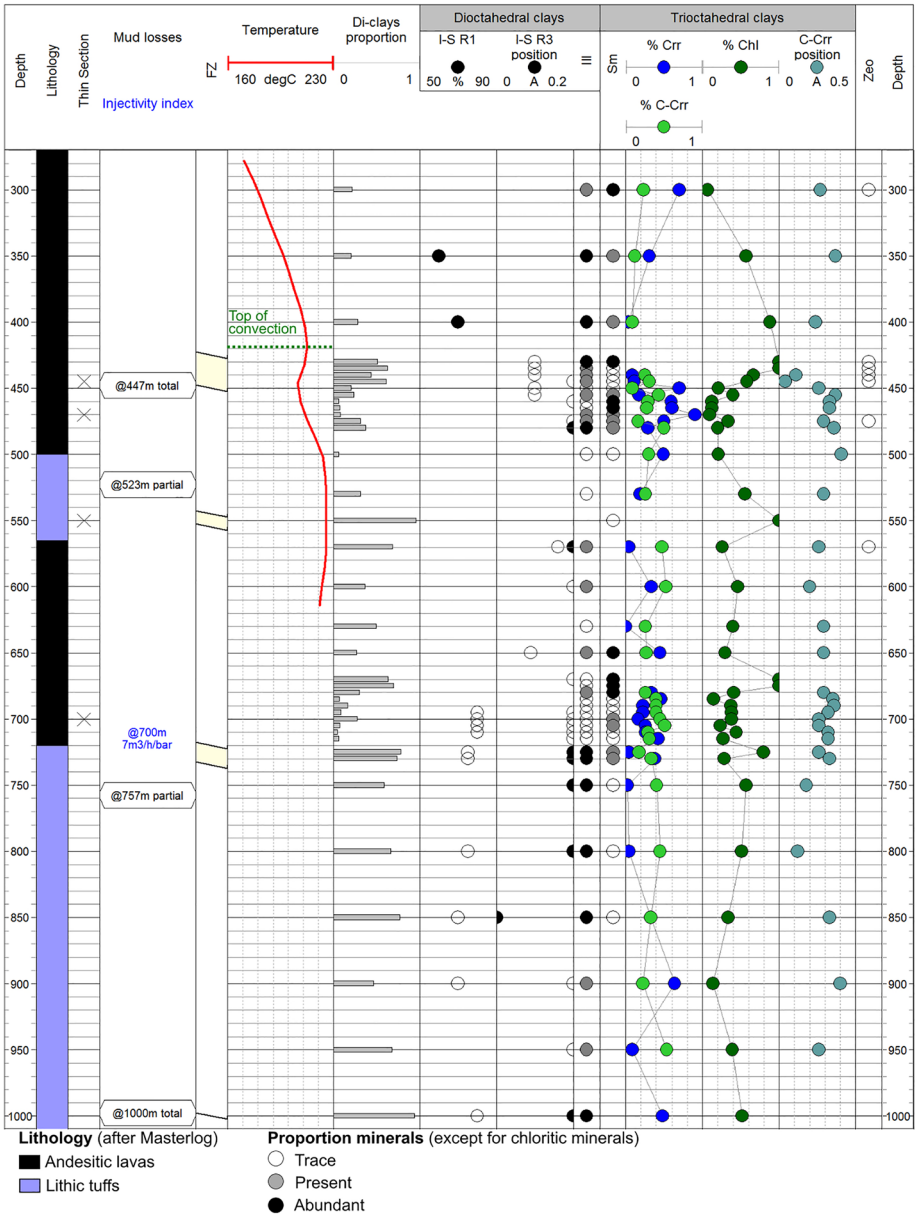

Fig. 2 Lithology, mud losses, measured injectivity index, permeable fracture and fault zones (FZ), temperature profile, and vertical distribution of hydrothermal minerals in CP5A well. Temperature profile was measured one year after drilling operations. The thickness and depth of the FZs are deduced from clay signature and thus are constrained by the sampling. Relative proportions of hydrothermal minerals are interpreted from EG-saturated XRD patterns (< 5 µm clay fraction). Di-clays proportion is the percentage of dioctahedral clay minerals (essentially illite and I-S) in the clay material. I-S R1 are expressed in percentage of smectite comprised between 60 and 90%. *C-Crr* chlorite/corrensite mixed layers, *Crr* corrensite, *Chl* chlorite, *Ill* illite, *I-S* illite–smectite mixed layers, *Sm* smectite, *Zeo* zeolites. Depth is expressed as Measured Depth

The temperature profile was not acquired below due to cement plug. The northern strand of the border fault is probably intersected at 1530 m depth in the dacitic tuffs. It is the main inflow of the well with an injectivity index of 10 m^3/h/bar. Partial mud losses were also observed at 925 m depth in the andesitic lavas at the top of the

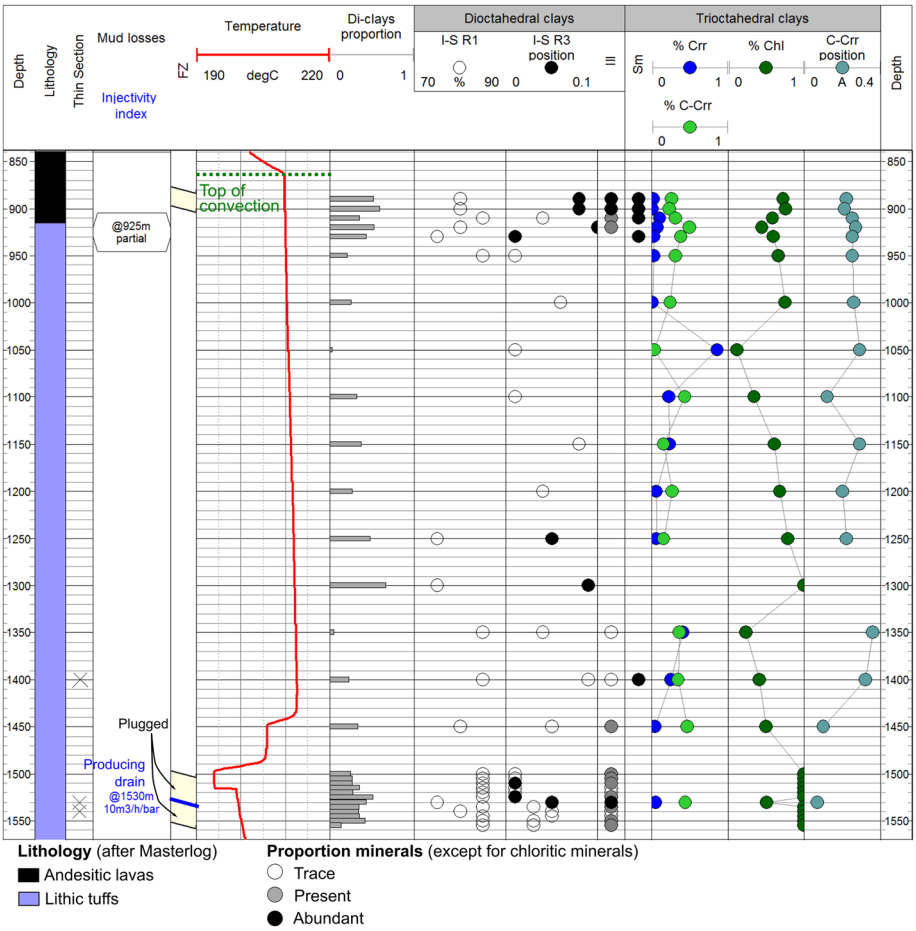

Fig. 3 Lithology, mud losses, measured injectivity index, permeable fracture and fault zones (FZ), temperature profile, and vertical distribution of hydrothermal minerals in CP2A well. Temperature profile was measured 10 months after drilling operations. The thickness and depth of the FZs are deduced from clay signature and thus are constrained by the sampling. Relative proportions of hydrothermal minerals are interpreted from EG-saturated XRD patterns (< 5 µm clay fraction). Di-clays proportion is the percentage of dioctahedral clay minerals (essentially illite and I-S) in the clay material. I-S R1 are expressed in percentage of smectite comprised between 70 and 90%. *C-Crr* chlorite–corrensite mixed layers, *Crr* corrensite, *Chl* chlorite, *Ill* illite, *I-S* illite–smectite mixed layers, *Sm* smectite. Depth is expressed as Measured Depth

convection. Production test of the well revealed a total fluid flow rate of 190 t/h with a wellhead pressure of 8 bar and a title of vapor of 7%.

In the present study, a special attention was paid to these two wells CP5A and CP2A because they both intersect the graben border fault. The tectonic control of the northern border fault on the characteristics of the hydrothermal alteration (alteration intensity, texture, and mineralogy) has been evaluated to explain the difference of productivity between both wells. If border fault was intersected in dacitic and lithic tuffs, both wells also intersect permeable FZs in andesitic lavas and this sampling will allow to discuss the lithological control on the hydrothermal flow.

Analytical methods

Petrographic investigations were carried out in 4 thin sections in CP5A well at 445, 470, 550, and 700 m depth (Fig. 2), observed under polarized microscope and scanning electron microscopy (SEM). Three thin sections were observed in CP2A well at 1400, 1530, and 1540 m depth, observed with same methodology (Fig. 3). As cutting samples present an average size between 0.5 and 2 mm, spatial resolution is low and textural relations between minerals are hardly observed.

Identification of clays and associated minerals was conducted by X-ray diffraction on the less than 5 µm fraction of the cutting material. Sampling was done in the reservoir zone marked by convection zone in the temperature profile. In CP5A well, 39 samples of cuttings were collected from 300 to 1000 m depth. The sampling was concentered around two FZ identified as permeable at 447 and 700 m depth. Samples below 1000 m depth were not available due to total loss of circulations. In CP2A well, 28 samples of cuttings from 890 to 1555 m depth were collected. The sampling was concentered at the top of reservoir zone around 900 m depth where partial mud losses occurred and around the main permeable FZ around 1530 m depth. Samples far from permeable zones in andesitic lavas and lithic tuffs were also selected as reference materials.

Cuttings samples were immersed in distilled water in the absence of preliminary grinding, and then disaggregated by ultrasonic treatment to properly disperse the clay particles in suspension. Oriented powders were prepared from sedimentation of the < 5 µm grain size clay separate of the suspension on glass slides. Clay minerals were identified by X-Ray Diffraction (XRD) of air-dried and ethylene–glycol (EG)-saturated oriented powders carried out on a Bruker D8 Advance diffractometer (CuKα radiation, 40 kV, 40 mA). The analytical conditions were as follows: angular domain: 2.5–30° 2θ; step increment: 0.025 2θ; and counting time per step: 3 s. Processing of the diffractometers was conducted using Match! Software (Crystal Impact). The clay minerals were identified according to Brindley and Brown (1980) (Fig. 4a and b). When mixed layers (I-S and/or C-Crr) were identified after EG saturation, the complex peaks between 7 and 10°2θ and 11 and 13°2θ were deconvoluted in Gaussian curves according to Lanson (1997) using the Fityk software (Wojdyr 2010). However, their study showed that consistent results can be obtained from different diffraction systems and numerical processing programs.

Details about the deconvolution method are explained in Vidal et al. (2022). The relative proportion of clay minerals species was evaluated from the area of the Gaussian curves after decomposition of the complex XRD peaks obtained for ethylene–glycol (EG)-saturated oriented powders (Fig. 4c):

A) The percentage of dioctahedral clay minerals in the bulk clay material (named *Di-clay proportion* in Figs. 2 and 3) was estimated from the areas of Gaussian curves. It consists in the following ratio: *(area I-S + area Ill)/(area I-S + area Ill + area Chl + area C-Crr + area Crr).*

B) The variation in relative proportion of illitic minerals, smectite, and zeolite was evaluated from the intensity of major XRD peaks: The higher the peak intensity, the higher the proportion of the mineral in the fine-grained fraction (Figs. 2 and 3). Regarding the clay minerals of the corrensite–chlorite series, the relative proportion

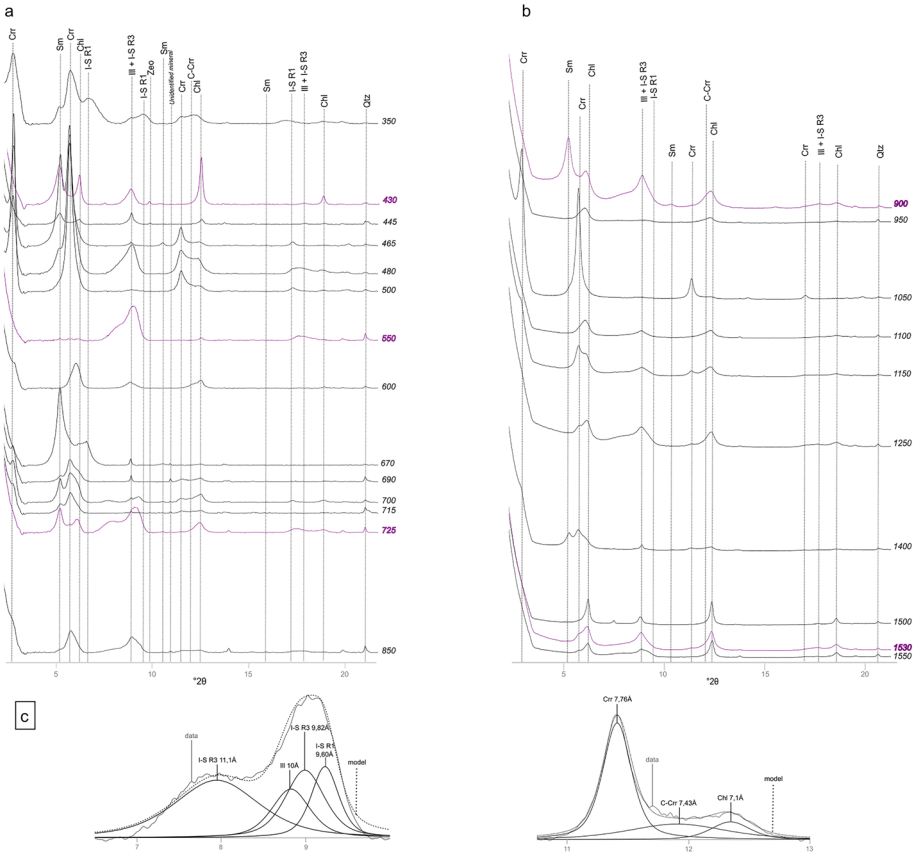

Fig. 4 X-ray diffractograms of EG-saturated oriented powder (< 5 µm clay fraction) **a** samples 350, 430, 445, 465, 480, 500, 550, 600, 670, 690, 700, 715, 725, and 850 in CP5A well **b** samples 900, 950, 1050, 1100, 1150, 1250, 1400, 1500, 1530, and 1550 in CP2A well. XRD in purple is associated to FZ **c** close-up on deconvolution of illitic peak for sample CP5A725 and of chloritic peak for sample CP5A465. *Chl* chlorite, *C-Crr* chlorite–corrensite mixed layers, *Crr* corrensite, *Ill* illite, *I-S* illite–smectite mixed layers, *Sm* smectite, *Qtz* quartz, Zeo: zeolites

of discrete chlorite intimately mixed with the clay minerals of the corrensite–chlorite series was calculated after peak deconvolution between 11 and 13°2θ, following the ratio: *%Chl = area Chl/(area Chl + area C-Crr + area Crr)*.

C) The percentage of illite component in the I-S mixed layers was estimated thanks to the position of the peak of I-S located between those of illite (d_{001}) and smectite (d_{002}), after decomposition of the complex peak between 7 and 10°2θ that occurs in the XRD pattern of EG-saturated oriented preparation. The closer the peak is from the theoretical position of illite (10 Å), the higher is the proportion of the illite component in the I-S mixed layer. In Figs. 2 and 3 I-S *R3 position* corresponds to the difference of d-spacing between the position of the peak of I-S R3 identified after deconvolution and the theoretical position of illite (10 Å). As it is comprised between 0.01 and 0.2 Å, the proportion of illite component within I-S is higher than 90% (Moore and Reynolds 1997).

The proportion of chlorite component within C-Crr mixed-layer minerals is estimated from the position of the C-Crr peak after deconvolution which may range from that of

discrete corrensite (7.75 Å) to that of discrete chlorite (7.1 Å) with as the amount of chlorite increases from 0 to 100% within the C-Crr mixed layer. The closer the peak is from the theoretical position of chlorite (7.1 Å), the higher is the proportion of chlorite in the C-Crr. The difference between the position of the peaks of C-Crr mixed-layer minerals and chlorite (determined after deconvolution) is named *C-Crr position* in Figs. 2 and 3. The 0.36–0.07 Å range of variation of C-Crr peak position so determined for all the analyzed samples indicates a variation from 50 to 90% in percentage of chlorite component in the C-Crr mixed layer.

Chemical compositions of primary and secondary minerals were acquired on thin sections of CP5A and CP2A wells using a SEM JEOL JSM-IT500 SEM equipped with a BRUKER lynxeye EDS associated with SPIRIT software at the IC2MP laboratory at the University of Poitiers. The analytical conditions were as follows: 15 kV; 1 nA; counting time: 50 s; and working distance: 11 mm. The analyzed elements were Si, Al, Fe, Mg, Mn, Ti, Ca, Na, and K. The system was calibrated with a variety of synthetic oxide and natural silicate standards. The reproducibility of the standard analyses is approximately 1%, except for Na, which had a reproducibility of 1.5%.

Alteration petrography

All samples collected in CPA5 and CPA2 wells show evidence of hydrothermal alteration involving the two main alteration styles (i.e., moderate pervasive alteration and fracture-controlled alteration) previously identified on the basis of petrographic and mineralogical criteria in CP4A and CP6A wells (Vidal et al. 2022).

Pervasive alteration has been observed everywhere, but it has been strongly obliterated by the fracture-controlled alteration close to the FZs. Pervasive alteration is particularly well expressed in the andesitic lavas and lithic tuffs located away from the main FZs. Regarding the clay mineralogy, pervasive alteration is characterized the replacement of the most of the original rock-forming mafic minerals (pyroxenes, volcanic glass, biotite) and, at a lesser degree, of igneous feldspars by a great variety of trioctahedral clay species ranging from saponite to chlorite through corrensite and chlorite–corrensite mixed layers. Such a variability in trioctahedral clay species may be observed both at the single sample scale (Fig. 5) and at the well scale (Figs. 2 and 3). Saponite is observed preferentially in replacement of orthopyroxenes (Fig. 5a) as well as the fine-grained material of the groundmass in the andesitic rocks, likely as replacement of volcanic glass in which it may be replaced by chloritic minerals (Fig. 5b). Chloritic minerals consist in intimate mixture of various proportions of chlorite, corrensite, and/or C-Crr and may be observed everywhere as replacing all types of mafic rock-forming minerals as well as infilling of dissolution voids (Fig. 5c, d and e). The fact that chloritic minerals may replace saponite in the altered pyroxenes or in the groundmass suggests that the trioctahedral clay minerals may have occurred sequentially during the progress of the pervasive alteration. Quartz, titanite, needle-shaped hematite, and calcite (Fig. 5e and f) are the most common non-clay minerals which crystallized in association with the trioctahedral clay minerals. Epidote has been uniquely observed near the bottom of CP2A well (below 1400 m depth). Numerous inclusions of arsenic minerals were observed in calcite and

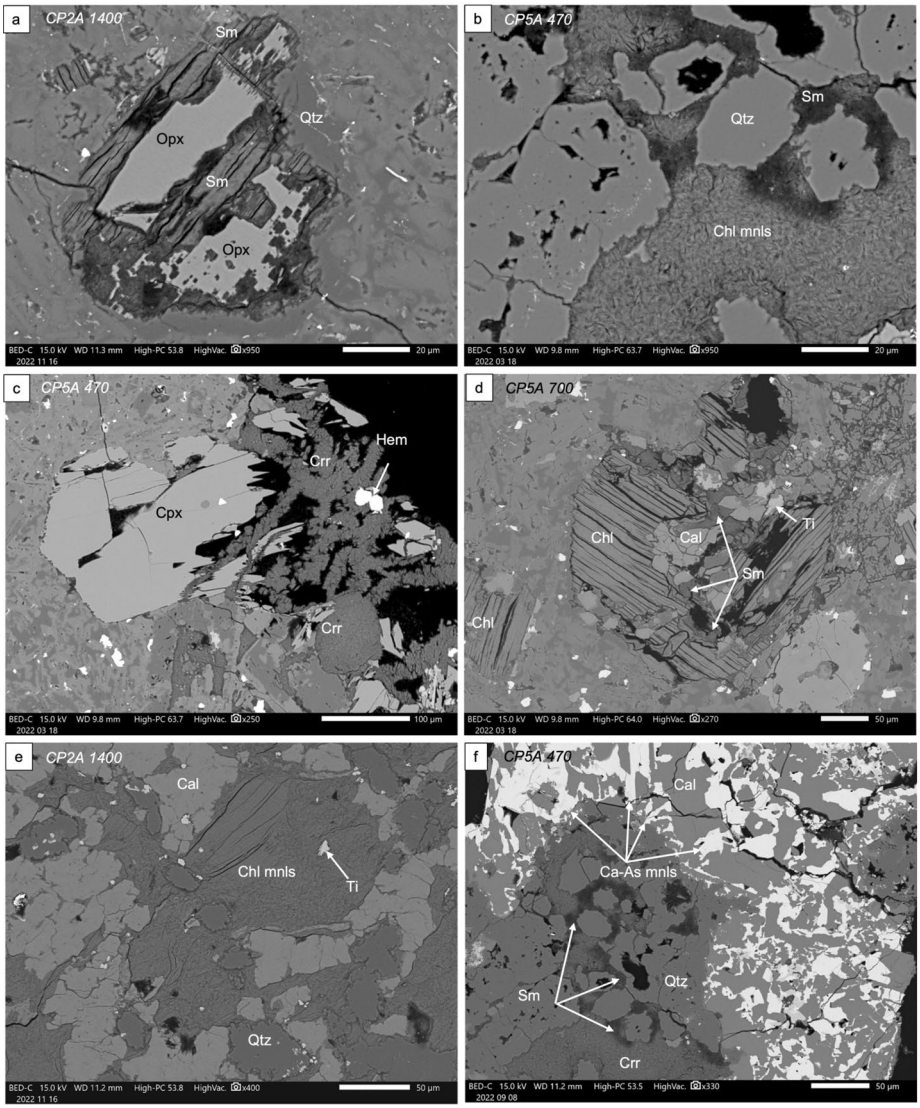

Fig. 5 SEM micrographs of volcanic rocks affected by pervasive hydrothermal alteration in both CP2A and CP5A wells of the CP geothermal system. **a** Igneous orthopyroxene (Opx) partly replaced by smectite (Sm) and quartz (Qtz) in altered andesitic tuffs sampled at 1400 m depth in CP2A well. **b** Groundmass replaced by quartz coexisting with chloritic minerals (Chl mnls) and minor smectite in altered andesitic lava sampled at 470 m depth in CP5A well. **c** Igneous clinopyroxene (Cpx) partly replaced by corrensite (Crr) and hematite (Hem) in altered andesitic lava sampled at 470 m depth in the CP5A well. **d** Mafic mineral of andesitic tuff (likely pyroxene) totally replaced by smectite, chlorite (Chl), calcite, and titanite (Ti) in altered andesitic lava sampled at 700 m depth in CP5A well. **e** Groundmass replaced by chloritic minerals, calcite, quartz, and minor titanite in altered andesitic tuffs sampled at 1400 m depth in CP2A well. **f** Groundmass replaced by corrensite, smectite, and quartz and by calcite with numerous inclusions of calcium-arsenic-bearing minerals (Ca–As mnls) in altered andesitic lava sampled at 470 m depth in CP5A well

quartz associated with trioctahedral clays, just below a fractured zone located at 470 m depth in CP5A well (Fig. 5f).

Fracture-controlled alteration is particularly developed close to the FZs, but it may be also observed locally farther, particularly in the dacitic tuffs, in superimposition over the

previously described pervasive alteration. Close to the major FZs, intense alteration is characterized by the destruction of the original texture of volcanic rocks due to the complete dissolution of the original igneous minerals (excepting quartz in dacitic rocks) and the cementation of the open spaces (cracks and dissolution voids) by potassic minerals essentially which nature and crystal chemical composition may have change with time.

The fracture-controlled alteration is clearly multi-event in the upper FZs between 440 and 550 m depth of CP5A well, where adularia precipitated in a first alteration stage was then partly replaced by K-rich phyllosilicates during a later alteration stage.

During the first alteration stage, the precipitation of adularia was massive, as microcrystalline aggregates in groundmass, and direct deposition from solutions into open spaces where it forms rhombic crystals (Fig. 6a and b). Quartz and calcite are frequently associated with adularia everywhere, whereas secondary albite was observed uniquely in replacement of igneous plagioclases. Specific texture of hydrothermal minerals in veins, such as flamboyant and feathery quartz, crustiform-collomorph bands, including quartz or chalcedony and adularia and blade shape calcite (Fig. 6c and d), are typical of precipitation from boiling fluids. Chemical zoning observed in rhombic crystals of adularia at the wall of open spaces (Fig. 6e) is indicative of periodic increase in Ba for K substitution in the crystal lattice during their crystal growth.

The second alteration stage is characterized by extensive crystallization of clay minerals of the illite group. In the altered rocks, illite and I-S were observed as infillings of open spaces that persisted after the earlier deposition of adularia and quartz (Fig. 6f), as replacement of igneous and hydrothermal feldspars and igneous biotite (Fig. 6g) and as veinlets infilling and wall rock alteration along microcracks. Minor amounts of chlorite have been observed in association with illite in vug infillings (Fig. 6f).

Adularia did not occur in the main FZs crosscut at greater depth in CP2A well. Alteration is characterized by destruction of the original texture of rocks as a result of the development of a vein network in strongly fractured rocks which suffered the dissolution of most of the igneous minerals and the secondary minerals of the earlier pervasive alteration (excepting quartz) and their replacement by illitic minerals, associated with quartz, calcite, and minor chlorite (Fig. 6h).

(See figure on next page.)

Fig. 6 SEM and optical microscope micrographs of volcanic rocks affected by fracture-controlled alteration in CP2A and CP5A wells of the CP geothermal system. **a** Massive crystallization of adularia (Adl) with minor albite (Alb) in altered dacitic tuffs sampled close to a major FZ at 445 m depth in CP5A well. SEM observations in backscattering mode evidence chemical zoning in K-feldspars related to solid solution between adularia and celsian (Ba-rich Adl). **b** Quartz (Qtz) and adularia veinlets in strongly altered dacitic tuffs sampled at 445 m depth in CP5A well with later illitization (Ill) of adularia and deposition of hematite (Hem) in the wall rock. **c** feathery texture of quartz crystallized in veins with calcite and adularia in strongly altered dacitic tuffs sampled at 445 m depth in CP5A well **d** Radial pattern of adularia needles typical of the flamboyant texture as fracture infillings in the dacitic tuffs sampled at 445 m depth in CP5A well. **e** Chemical zoning related to Ba for K substitution in outer part of adularia crystals at the wall of the open spaces in the strongly altered dacitic tuffs sampled at 445 m depth in CP5A well. **f** Late crystallization of illite (Ill), chlorite (Chl), and hematite (Hem) after deposition of adularia and quartz in the strongly altered dacitic tuffs sampled at 445 m depth in CP5A well. **g** Dissolution of adularia crystals followed by crystallization of illitic clay minerals in the dacitic tuffs sampled at 550 m depth in CP5A well. **h** Quartz-hematite veinlets with intense alteration in wall rock consisting in the replacement of andesitic tuffs by illitic minerals and carbonates (calcite with minor inclusions of dolomite), close to a major FZ at 1540 m in CP2A well

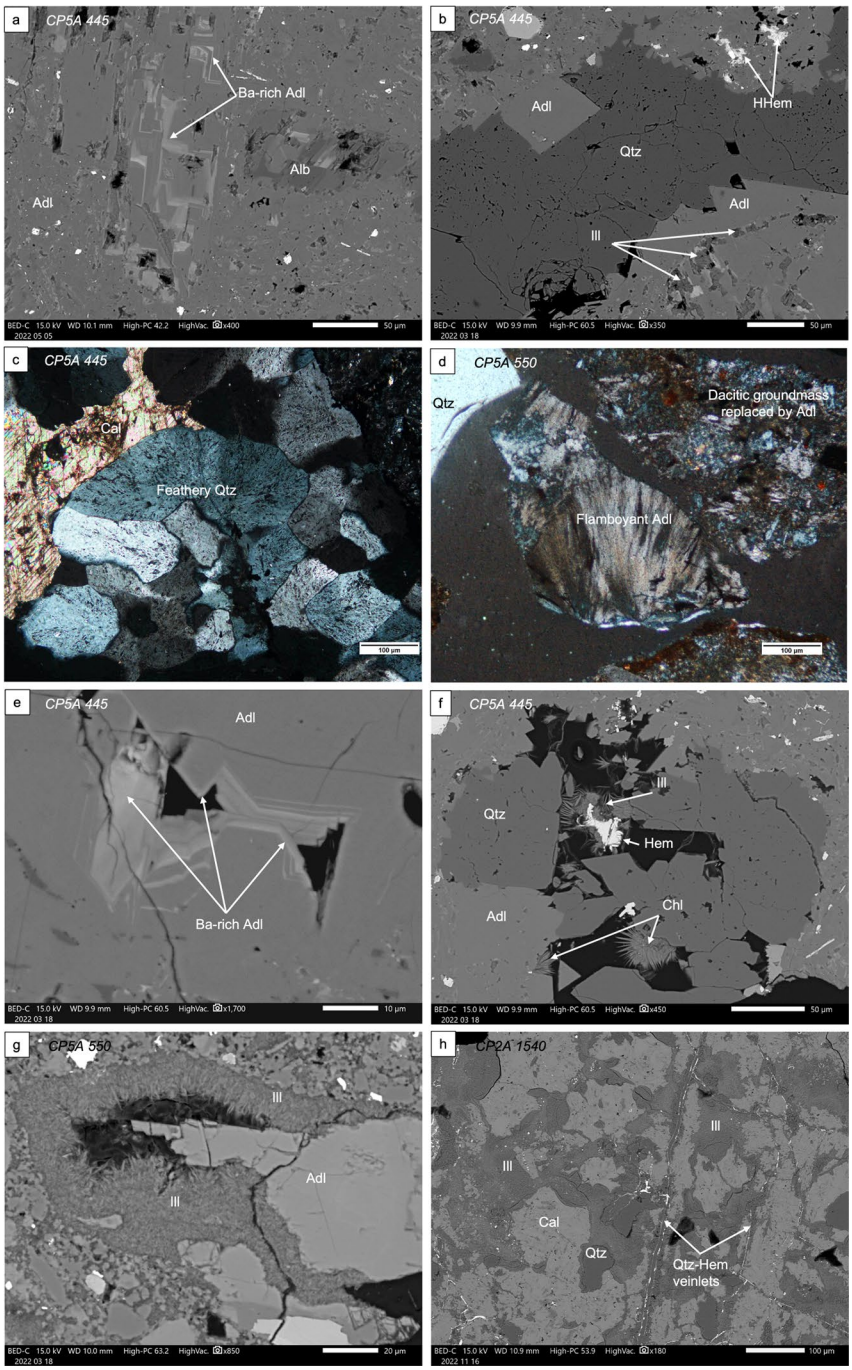

Fig. 6 (See legend on previous page.)

Farther from main FZs, the fracture-controlled alteration is characterized by weak to moderate replacement of feldspars (phenocrysts and groundmass) by illitic minerals, calcite, and minor quartz.

Vertical distribution of hydrothermal minerals

According to petrographic observations most of trioctahedral clay minerals (i.e., saponite, corrensite, mixed chlorite–corrensite layers, and chlorite) identified in both wells occurred as alteration products from a pervasive alteration (excepting small amounts of chlorite that may be related to fracture-controlled alteration, as shown in Fig. 6F). From XRD mineral identification in both wells (Figs. 2, 3, and 4), it appears that (1) minerals of trioctahedral clay series are present throughout (although they are less abundant in areas where pervasive alteration has been strongly obliterated by fracture-controlled alteration), and (2) several mineral types of the trioctahedral clay sequence coexist at any depth. Therefore, regarding the pervasive alteration, there is no clear evidence of depth- or temperature-related variation in the mineralogy of the clay minerals. For instance, saponite has been identified in presence of chlorite, corrensite, and/or C-Crr in many samples collected at depth between 300 and 1400 m. At the most one can note a rough trend to decreasing content of the highly expandable minerals (saponite, corrensite) in the total amount of trioctahedral clays with increasing depth (Fig. 4). The fact that chlorite is the predominant type trioctahedral clay minerals in rocks in which illitic minerals predominate (Figs. 2 and 3), suggesting that this chlorite is related to fracture-controlled alteration (as shown in Fig. 6f). In highly illitized samples of the main producing drain of the FZ crosscut between 1500 and 1550 m depth in CP2A well, the amount of chloritic minerals is too small to allow their identification by XRD.

Clays of the dioctahedral sequence are products of the fracture-controlled alteration and consist uniquely in K-bearing minerals (i.e., I-S and discrete illite). I-S R1 (with smectite between 60 and 80%) were identified mainly at shallow depths, above 400 m depth in CP5A well. These mixed-layer minerals are particularly abundant above the top of the fluid convective zone where temperature is lower than 200 °C (Fig. 2). They are scarcely observed below in association with I-S R3 (Figs. 2 and 3). I-S R3 (with ill > 90%) and illite are closely associated in both CP5A and CP2A wells in depths where a very weak thermal gradient is observed traducing convective heat transfer. In CP5A well, the percentage of dioctahedral clays in bulk clay material is particularly high (higher than 50%) in the FZ as well as in lithic tuffs intersected below 720 m depth (Fig. 2). In CP2A well, the highest percentages of dioctahedral clays were observed in the FZs and also in the lithic tuffs next to 1300 m depth (Fig. 3).

Zeolites from with heulandite-clinoptilolite group according to a reflection peak at 8.95–8.96 Å in the oriented XRD are scarcely observed above 600 m depth of CP5A well. They are a minor alteration minerals that were not observed by petrographic and chemical microanalyses.

Chemistry of hydrothermal minerals

Chemical analyses of hydrothermal minerals conducted on thin sections of CP5A and CPA2 wells are presented in Additional file 1.

Most of the trioctahedral smectites have a chemical composition which agree with that of high-charge saponite, with interlayer charge ranging from 0.5 to 0.8 per O_{10} $(OH)_2$, and XFe ratio (Fe/(Fe + Mg)) ranging between 0.12 and 0.37 likely related to the chemistry of the mineral that they are replacing (Additional file 1: Table S1). The small amount

of chemical analyses which differ by a lower interlayer charge coupled with octahedral occupancy higher than 3 atoms are indicative of intimate mixture of saponite with minor amounts of chloritic minerals (Fig. 5b).

The compositional field of the chloritic minerals analyzed in both wells is wide and spread over clay species from corrensite to chlorite through C-Crr (Fig. 7a). From a crystallochemical point of view, corrensite-to-chlorite transition is marked by a strong increase of the iron content at the expense of the magnesium content in the octahedral sheets; XFe increases from 0.1 to 0.47 from corrensite to chlorite (Additional file 1: Tables S2, S3 and Fig. 7a).

The chemical compositions of chlorite are very homogeneous throughout CP5A and CP2A wells (Additional file 1: Table S3). In contrast to what was observed in CP6A and CP4A wells, no Fe-rich chlorite (XFe > 50) was analyzed in association with illite (Fig. 7a) (Vidal et al. 2022). The chemical composition of the few chlorites analyzed in samples of CP5A well in which illite replaced adularia is similar of chlorite from the pervasive alteration.

The chemical composition of illitic minerals which are related to fracture-controlled alteration in both wells agree with those of mixture of I-S and illite (Additional file 1: Table S4). The interlayer charge of these clay minerals is essentially satisfied by potassium

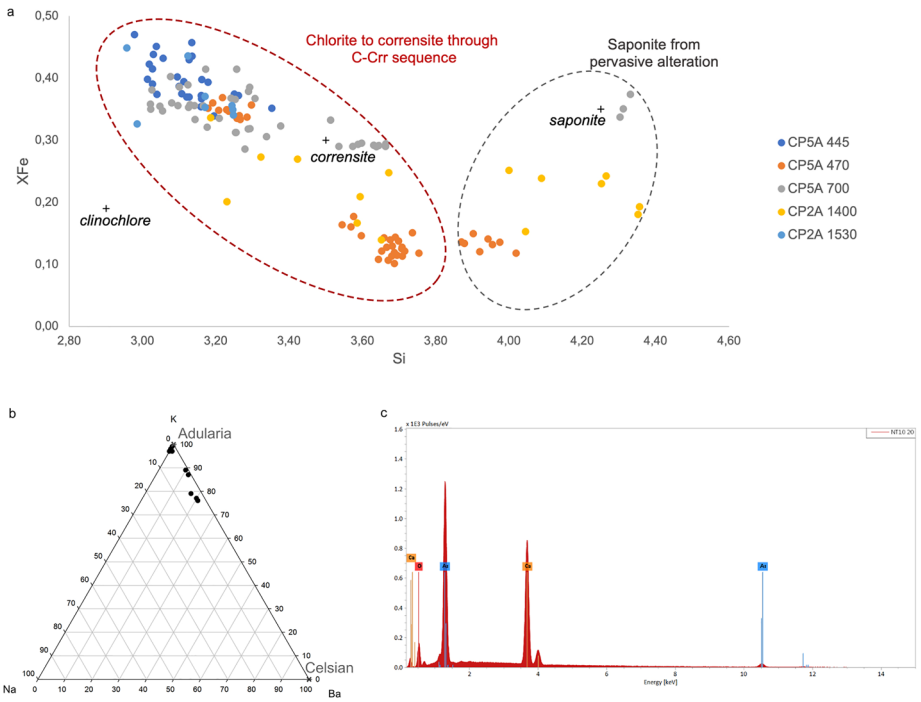

Fig. 7 **a** Plot of structural formulae of trioctahedral clays in a diagram of XFe versus Si for CP5A and CP2A wells (XFe = Fe/(Fe + Mg). The average structural formulae are presented in Additional file 1: Tables S1, S2, S3. In this figure all the samples are represented with a relative structure containing 14 oxygen atoms and assuming that the total iron content was composed of Fe2 + . Theoretical compositions of clinochlore, corrensite, and saponite are provided for reference. **b** Chemical compositions of K-rich and Ba-rich feldspars at 445 m depth in CP5A well plotted in a Na–K-Ba ternary diagram. Representative analyses are described in Table 1. Theoretical compositions of adularia and celsian are given for reference (crosses). **c** representative SEM–EDS spectrum of calcium arsenate mineral observed at 470 m depth in CP5A well

and varies from less than 0.7 to more than 0.9 according to the relative amounts of illite vs I-S. There is no evidence of depth-related compositional variation in illitic minerals. The particularly high interlayer charges (0.90–1) observed in illitic minerals which replace adularia at 445 and 470 m depth in CP5A well are likely due to the persistence of adularia impurities within the clay material (Fig. 6g).

Chemical microanalyses conducted on adularia crystals in the wall of open spaces of strongly altered dacitic tuffs at 445 m depth in CP5A well (Fig. 6e) reveal compositional variations between 100% adularia ($Si_3Al_1K_1O_8$) and 75% adularia–25% celsian ($Si_{2.75}Al_{1.25}K_{0.75}Ba_{0.25}O_8$) (Table 1 and Fig. 7b).

Chemical compositions of inclusions of arsenic minerals observed at 470 m depth in CP5A well (Fig. 5f) indicate a Ca/As ratio of 2/3 which is characteristic of minerals of the calcium arsenate group $Ca_3(AsO_4)_2$ nH_2O (with $n=0$–11) as reported in literature (Majzlan et al. 2014).

Discussion

These results of hydrothermal alteration in CP5A and CP2A wells evidence a high heterogeneity as already noticed in CP4A and CP6A wells (Vidal et al. 2022). Moreover, original results from CP5A and CP2A allow us to identify, at least, three distinct hydrothermal events, spatially and temporary superimposed. A fracture-controlled event related to boiling processes was not evidenced previously and suggests a strong control of the eastern border fault on reservoir productivity. However, this control remains at the South of Pabellón dome.

A multi-event hydrothermal alteration

Pervasive alteration event

A pervasive alteration associated to *trioctahedral clays (saponite, corrensite, C-Crr, and Fe–Mg chlorite) + hematite + calcite* is observed in all samples of CP5A and CP2A wells but is well expressed far from FZs. Zeolites from heulandite-clinoptilolite group are scarcely observed in CP5A well. Epidote is observed at the bottom of CP2A well underlining a hotter old temperature of the geothermal field that is probably cooling far from main permeable structures. This pervasive alteration was already observed in CP4A and CP6A wells (Vidal et al. 2022). It is a propylitic alteration very common during

Table 1 Representative structural formulas for Ba-rich K-feldspar (Fsp) and adularia (Adl) at 44 5 m depth in CP5A well

%atom	Ba-rich Fsp	Adl
Si	2.74	3.01
Al	1.27	0.99
K	0.74	0.99
Ba	0.23	0.00
Fe^{3+}	0.00	0.00
Mg	0.00	0.00
Ti	0.00	0.00
Mn	0.00	0.00
Na	0.04	0.01
Ca	0.00	0.00

cooling of magmatic intrusive bodies resulting from interactions between igneous minerals with stagnant fluids of diverse in pores or microcracks (Lowell and Guilbert 1970; Thomasson and Kristmannsdottir 1972). In the context of andesitic volcanism, it is mainly dominated by trioctahedral clays and is representative of hydrothermal alteration in inactive flow regimes (Beaufort et al. 1990). Occurrences of hematite in which iron is essentially in the ferric state is indicative of crystallization in oxidizing condition. The chemistry of chloritic minerals is rock dominated during propylitic alteration and they are preferentially magnesium rich (i.e., $Fe/Fe+Mg<0.5$) because they incorporate iron essentially at the ferrous state under oxidizing conditions (Beaufort et al. 1992; López-Munguira et al. 2002; Mas et al. 2006).

Fracture-controlled event related to illitization

A fracture-controlled event is mostly associated to a strong illitization. In fact, the same mineralogical paragenesis *illite + I-S R3 (ill > 90%) + carbonates (mainly calcite) + chlorite in minor amount* is observed in all permeable FZs of CP5A and CP2A wells. Morphology of clays observed in permeable FZs suggests abrupt changes in the flow regime, such as mixing of geothermal fluids that lead to explosive nucleation of small clay crystallites, and promotes occurrences of heterogeneous mineral assemblages, such as I-S. This alteration event is related to near neutral K-rich fluid ranging from 200 °C to 300 °C with high CO_2 content as known in the present geothermal reservoir and confirmed by the presence of calcite as hydrothermal precipitated phase. This clay signature is the same than the one already observed in CP4A and CP6A wells (Vidal et al. 2022). However, chlorite is less abundant in FZs of CP5A and CP2A wells and Fe-rich composition was not clearly observed.

Fracture-controlled event related to boiling processes

Another fracture-controlled event is dominated by *adularia + Ba-rich feldspar + silica polymorphs (quartz, chalcedony) + calcium arsenates + calcite + illite*. It was observed in shallow permeable FZs of CP5A well, that are possibly at a liquid/steam interface at about 4100 m a.s.l., i.e., 400 m depth (Baccarin et al. 2021). Adularia, blade shape calcite, quartz, chalcedony, and their flamboyant, feathery, and crustiform-collomorph textures suggest boiling processes that were already mentioned in PAE-1 well (Urzúa et al. 2002). Calcium arsenates are also observed at 470 m depth. These hydrothermal parageneses are common in low-sulfidation epithermal deposits reported in the literature (Dong et al. 1995; Dong and Morrison 1995; Patrier et al. 2013; Rowland and Simmons 2012; Simmons and Browne 2000). Boiling is inferred to be the most common depositional mechanism of these minerals that grow under conditions of high supersaturation in response to rapidly changing conditions at temperatures. At the end of boiling processes, when pressure increases and pH decreases, illite with a very high interlayer charge (close to mica) can locally and temporarily precipitate until another boiling event occurs. The fact that these minerals assemblages are observed in CP5A well could be linked to the intersection of the graben border fault that allows unimpeded fluid upflow.

These three alteration events can be spatially and temporarily superimposed. The propylitic alteration probably started before but continues even if locally in the permeable levels, a multi-event fracture-controlled alteration occurred erratically. Minerals

parageneses precipitate under different states of pressure, pH, f_{O2}, and temperature one after the other and can strongly obliterate previous hydrothermal former minerals. Clay parageneses are observed together everywhere in the reservoir and do not follow a continuous evolution with depth and temperature. They seem more influenced by kinetics than temperature evolution in the reservoir as already observed by Berger et al. (2018), Robinson et al. (2002), and Escobedo et al. (2021) among others.

Structural control of the graben fault

Our observation of boiling process is clearly restricted to the major upflow zone of the reservoir above the eastern border fault south of the Pabellón dome. It suggests that the eastern border fault acts as a preferential pathway for unimpeded fluid flow. However, its control seems limited to south of the Pabellón dome as mineralogical indicators are very different at the north. In CP2A well, the permeability of the northern strand intersected between 1500 and 1555 m depth was likely reduced by an intense illitization. The actual fluid circulation seems restricted at 1530 m depth. This hypothesis is supported by the absence of mud losses and relatively low injectivity index. Moreover, the median strand of the fault might be intersected around 1100 m depth as in the twin well CP2 located few meter away with the same vertical trajectory (Baccarin et al. 2021). Clay pattern suggests a significant amount of dioctahedral clays between 1100 and 1300 m depth and evidence of permeability does not allow to infer where the median strand was intersected in CP2A well.

This heterogeneity in terms of permeability and fluid flow along a fault zone was already described in the literature (Caine et al. 2010; Faulkner et al. 2011; Vidal et al. 2017). A fault structure observed at seismic scale is in reality often divided over several strands that act as individual slip surfaces at sub-seismic scale. Such a complex architecture might be reservoir–reservoir juxtapositions across individual fault strands that behave as combined conduit-barrier (Faulkner et al. 2010). Fluid flow around a fault zone can be dominated not only by a small number of fractures interconnected in the surrounding damage zone but also by the nature and amount of secondary deposits, such as phyllosilicates, that can sealed potential pathways for fluid (Caine et al. 1996).

Abundance of dioctahedral clays in tuffs compared to lavas could suggest a lithological control. Because of their primary porosity, tuffs are better candidates for fluid circulations than welded lavas. However, even outside the graben, in tuffs intersected by CP4A well, the trioctahedral sequence is dominant away from permeable FZs. Thus, hydrothermal alteration seems more influenced by permeable FZs that channelized fluid circulations than primary porosity.

The present study improves the conceptual model previously proposed in the literature of the CP geothermal field. Illitization is considered as permeability signature of actual fluid circulations in the fracture network developed inside and outside the graben (Vidal et al. 2022). Original results from CP5A and CP2A wells not only confirm this observation but also highlight a specific signature of the eastern border fault. The epithermal deposits at shallow FZs suggest unimpeded fluid circulations under boiling context that support the important productivity index observed in CP5A well. These epithermal deposits are not observed at the north of Pabellón dome where the illitization is dominant in CP2A well suggesting clogging of natural permeability

of the fault and supporting the low productivity index of the well. Thus, the eastern border fault is spatially and temporarily heterogeneous. It is a complex structure that clearly influences the geodynamics of actual hydrothermal circulations and the geometry of the hot core of the reservoir.

Conclusion

Fluid circulations of CP reservoir are channelized by a wide fracture network connected to the eastern border fault. The latter controls the narrow thermal plume promoting focused vertical fluid flow at south of the Pabellón dome. Hydrothermal fluids that have circulated or actively circulate undergo abrupt oversaturation conditions that are conductive to two phenomena:

- Boiling and epithermal deposits (adularia, Ba-rich feldspar, feathery quartz, chalcedony, and calcium arsenates) evidenced in the shallow FZs of the reservoir,
- Mixing of fluids with contrasting temperatures and distinctive illitization (I-S R3 with ill > 90% and illite) observed in all permeable FZs of the reservoir.

Moreover, a pervasive alteration dominated by trioctahedral clays are observed away from FZs. Superimposition of these alteration processes produce inherent heterogeneity of hydrothermal deposits and complex evolution of hydrothermal flow paths. At north of the Pabellón dome, hydrothermal activity collapsed in response to intense illitization which plugged the permeable fault zone. As exploitation of the geothermal system leans on well-connected fracture network providing sufficient permeability, the study of hydrothermal alteration should be extended to other wells in order to characterize at best the hydrothermal flow at the CP geothermal field.

Supplementary Information

The online version contains supplementary material available at https://doi.org/10.1186/s40517-023-00260-8.

Additional file 1: Chemistry of clay minerals in CP5A and CP2A wells Table S1. Structural formula of saponite at 470 and 700 m in CP5A well and at 1400 m depth in CP2A well. n.a.: number of analyses; an. ave.: analytical average; s.d.: standard deviation. OCT: octahedral occupancy; INTCH: interlayer charge;. The formulas are normalized to 11 O atoms and total Fe is considered as Fe^{2+}. **Table S2.** Structural formula of corrensite and C-Crr mixed layers at 470 and 700 m depth in CP5A well and C-Crr mixed layers at 1400 m depth in CP2A. n.a.: number of analyses; an. ave.: analytical average; s.d.: standard deviation. OCT: octahedral occupancy; INTCH: interlayer charge;. The formulas are normalized to 25 O atoms and total Fe is considered as Fe^{2+}. **Table S3.** Structural formula of chlorite at 445 and 700 m depth in CP5A well and 1400, 1530 and 1540 m depth in CP2A well. n.a.: number of analyses; an. ave.: analytical average; s.d.: standard deviation. OCT: octahedral occupancy; INTCH: interlayer charge;. The formulas are normalized to 14 O atoms and total Fe is considered as Fe^{2+}. **Table S4.** Structural formula of illitic minerals at 445 m, 470 m, 550 m and 700 m depth in CP5A well and 1530 and 1540 m depth in CP2A well. n.a.: number of analyses; an. ave.: analytical average; s.d.: standard deviation. OCT: octahedral occupancy; INTCH: interlayer charge;. The formulas are normalized to 11 O atoms and total Fe is considered as Fe^{3+}.

Acknowledgements

The authors thank Geotérmica del Norte (GDN) for authorizing the use of wells data of Cerro Pabellón Power Plant project.

Author contributions

JV and DM conceptualized the study and acquired funding for it. GR and GV made the data available and shared their knowledge about the CP geothermal field. JV and SM participated to field work. JV, PP, DB, and SM performed the laboratory work on cuttings samples and data analysis. JV wrote the original draft, and all the authors approved the final manuscript.

Funding
This study has benefited the scientific and financial support of the Andean Geothermal Center of Excellence (CEGA), Anid-Fondap projects #15090013, 15200001 & ACE210005. This study was published in the framework of the ANID-Fondecyt postdoctoral Grant No 3210150 attributed to J. Vidal.

Availability of data and materials
Not applicable.

Declarations

Competing interests
The authors declare that they have no known competing financial interests or personal relationships that could have appeared to influence the work reported in this paper.

Received: 7 January 2023 Accepted: 12 June 2023
Published: 29 June 2023

References

Aguirre I, Clavero J, Simmons S, Giavelli A, Mayorga C, Soffia JM. "Colpitas"—a new geothermal project in Chile. Geotherm Resour Counc Trans. 2011;35:1141–5.
Aravena D, Muñoz M, Morata D, Lahsen A, Parada MÁ, Dobson P. Assessment of high enthalpy geothermal resources and promising areas of Chile. Geothermics. 2016;59:1–13. https://doi.org/10.1016/j.geothermics.2015.09.001.
Arcos R, Clavero J, Giavelli A, Simmons SF, Aguirre I, Martini S, Mayorga C, Pineda G, Parra J, Soffia JM. Surface exploration at pampa lirima geothermal project, Central Andes of Northern Chile. Geotherm Resour Counc Trans. 2011;35:689–93.
Baccarin F, Volpi G, Rivera G, Giorgi N, Arias A, Giudetti G, Cei M, Cecioni M, Rojas L, Ramirez C. Cerro Pabellón geothermal field (Chile): geoscientific feature and 3D geothermal model, in: proceeding of the World Geothermal Congress 2020+1. Reykjavik, Iceland; 2021.
Beaufort D, Westercamp D, Legendre O, Meunier A. The fossil hydrothermal system of Saint Martin, Lesser Antilles: geology and lateral distribution of alterations. J Volcanol Geoth Res. 1990;40:219–43. https://doi.org/10.1016/0377-0273(90)90122-V.
Beaufort D, Patrier P, Meunier A, Ottaviani MM. Chemical variations in assemblages including epidote and/or chlorite in the fossil hydrothermal system of Saint Martin (Lesser Antilles). J Volcanol Geoth Res. 1992;51:95–114. https://doi.org/10.1016/0377-0273(92)90062-I.
Berger G, Beaufort D, Antoine R. Clay minerals related to the late magmatic activity of the Piton des Neiges (Réunion Island): consequence for the primitive crusts. Clay Miner. 2018;53:675–90. https://doi.org/10.1180/clm.2018.51.
Brindley GW, Brown G. X-ray diffraction procedures for clay mineral identification. In: Brindley GW, Brown G, editors. Crystal structures of clay minerals and their X-Ray identification. London, Great Britain: Mineralogical Society; 1980. p. 305–60.
Caine JS, Evans JP, Forster CB. Fault zone architecture and permeability structure. Geology. 1996;24:1025–8. https://doi.org/10.1130/0091-7613(1996)024%3c1025:FZAAPS%3e2.3.CO;2.
Caine JS, Bruhn RL, Forster CB. Internal structure, fault rocks, and inferences regarding deformation, fluid flow, and mineralization in the seismogenic Stillwater normal fault, Dixie Valley, Nevada. J Struct Geol. 2010;32:1576–89. https://doi.org/10.1016/j.jsg.2010.03.004.
Cappetti G, Giorgi N, Arias A, Volpi G, Rivera G, Cei M, Fedeli M, Di Marzio G, Pasti M, Massei S, Baccarin F. The Cerro Pabellón geothermal project (Chile): from surface exploration to energy production, in: proceeding of the World Geothermal Congress 2020+1. Reykjavik, Iceland; 2021.
Cumming WB, Vieytes H, Ramírez C, Sussman D. Exploration of the la torta geothermal prospect, Northern Chile. Geotherm Resour Counc Trans. 2002;26:3–7.
Dong G, Morrison GW. Adularia in epithermal veins, Queensland: morphology, structural state and origin. Mineral Deposita. 1995;30:11–9. https://doi.org/10.1007/BF00208872.
Dong G, Morrison G, Jaireth S. Quartz textures in epithermal veins, Queensland—classification, origin, and implication. Econ Geol. 1995;90:1841–56. https://doi.org/10.2113/gsecongeo.90.6.1841.
Escobedo D, Patrier P, Beaufort D, Gibert B, Levy L, Findling N, Mortensen A. Contribution of the paragenetic sequence of clay minerals to re-examination of the alteration zoning in the Krafla geothermal system. Minerals. 2021;11:935. https://doi.org/10.3390/min11090935.
Faulkner DR, Jackson CAL, Lunn RJ, Schlische RW, Shipton ZK, Wibberley CAJ, Withjack MO. A review of recent developments concerning the structure, mechanics and fluid flow properties of fault zones. J Struct Geol. 2010;32:1557–75. https://doi.org/10.1016/j.jsg.2010.06.009.
Faulkner DR, Mitchell TM, Jensen E, Cembrano J. Scaling of fault damage zones with displacement and the implications for fault growth processes. J Geophys Res Solid Earth. 2011. https://doi.org/10.1029/2010JB007788.
Flexser S. Hydrothermal alteration and past and present thermal regimes in the western moat of Long Valley caldera. J Volcanol Geoth Res. 1991;48:303–18. https://doi.org/10.1016/0377-0273(91)90048-5.
Giordano G, Pinton A, Cianfarra P, Baez W, Chiodi A, Viramonte J, Norini G, Groppelli G. Structural control on geothermal circulation in the Cerro Tuzgle-Tocomar geothermal volcanic area (Puna plateau, Argentina). J Volcanol Geoth Res. 2013;249:77–94. https://doi.org/10.1016/j.jvolgeores.2012.09.009.
Giudetti G, Tempesti L. First Geochemical data from Cerro Pabellón geothermal project (Apacheta Region, Chile), in: proceeding of the World Geothermal Congress 2020+1. Reykjavik, Iceland; 2021.

Godoy B, Wörner G, Kojima S, Aguilera F, Simon K, Hartmann G. Low-pressure evolution of arc magmas in thickened crust: the San Pedro-Linzor volcanic chain, Central Andes, Northern Chile. J S Am Earth Sci. 2014;52:24–42. https://doi.org/10.1016/j.jsames.2014.02.004.

Inoue A, Kitagawa R. Morphological characteristics of illitic clay minerals from a hydrothermal system. Am Miner. 1994;79:700–11.

Lanson B. Decomposition of experimental X-Ray diffraction patterns (profile fitting): a convenient way to study clay minerals. Clays Clay Miner. 1997;45:132–46. https://doi.org/10.1346/CCMN.1997.0450202.

Legault JM, Lombardo S, Zhao S, Clavero J, Aguirre I, Arcos R, Lira E. ZTEM airborne AFMAG EM and ground geophysical survey comparisons over the pampa lirima geothermal field in Northern Chile. Geotherm Resour Counc Trans. 2012;36:1001–1008.

López-Munguira A, Nieto F, Morata D. Chlorite composition and geothermometry: a comparative HRTEM/AEM-EMPA-XRD study of Cambrian basic lavas from the Ossa Morena Zone, SW Spain. Clay Miner. 2002;37:267–81. https://doi.org/10.1180/0009855023720033.

Lowell JD, Guilbert JM. Lateral and vertical alteration-mineralization zoning in porphyry ore deposits. Econ Geol. 1970;65:373–408. https://doi.org/10.2113/gsecongeo.65.4.373.

Majzlan J, Drahota P, Filippi M. Parageneses and crystal chemistry of arsenic minerals. Rev Mineral Geochem. 2014;79:17–184. https://doi.org/10.2138/rmg.2014.79.2.

Mas A, Guisseau D, Patrier Mas P, Beaufort D, Genter A, Sanjuan B, Girard JP. Clay minerals related to the hydrothermal activity of the Bouillante geothermal field (Guadeloupe). J Volcanol Geoth Res. 2006;158:380–400. https://doi.org/10.1016/j.jvolgeores.2006.07.010.

Maza SN, Collo G, Morata D, Lizana C, Camus E, Taussi M, Renzulli A, Mattioli M, Godoy B, Alvear B, Pizarro M, Ramírez C, Rivera G. Clay mineral associations in the clay cap from the Cerro Pabellón blind geothermal system, Andean Cordillera, Northern Chile. Clay Miner. 2018;53:117–41. https://doi.org/10.1180/clm.2018.9.

Maza SN, Collo G, Morata D, Cuña-Rodriguez C, Taussi M, Renzulli A. The hydrothermal alteration of the Cordón de Inacaliri volcanic complex in the framework of the hidden geothermal systems within the Pabelloncito Graben (Northern Chile). Minerals. 2021a;11:1279. https://doi.org/10.3390/min11111279.

Maza SN, Collo G, Morata D, Taussi M, Vidal J, Mattioli M, Renzulli A. Active and fossil hydrothermal zones of the Apacheta volcano: insights for the Cerro Pabellón hidden geothermal system (Northern Chile). Geothermics. 2021;96:102206. https://doi.org/10.1016/j.geothermics.2021.102206.

Moore DM, Reynolds RC. Identification of clay minerals and associated minerals. 2nd ed. Oxford, New-York: Oxford University Press; 1997.

Morata D, Reich M, Muñoz-Saez C, Daniele L, Rivera G, Volpi G, Cecioni M, Giudetti G, Cappetti G. Origin and age of fluids at the Cerro Pabellón geothermal system, Northern Chile, in: Proceedings 41st New Zealand Geothermal Workshop. Auckland, New Zealand; 2019.

Morata D, Aravena D, Lahsen A, Muñoz M, Valdenegro P. Chile Up-Date: The First South American geothermal power plant after one century of exploration, in: Proceeding of the World Geothermal Congress 2020+1. Reykjavik, Iceland; 2021.

Patrier P, Papapanagiotou P, Beaufort D, Traineau H, Bril H, Rojas J. Role of permeability versus temperature in the distribution of the fine (< 0.2 µm) clay fraction in the Chipilapa geothermal system (El Salvador, Central America). J Volcanol Geoth Res. 1996;72:101–20. https://doi.org/10.1016/0377-0273(95)00078-X.

Patrier P, Bruzac S, Pays R, Beaufort D, Bouchot V, Verati C, Gadalia A. Occurrence of K-feldspar-bearing hydrothermal breccias in the Bouillante geothermal field (Basse Terre – Guadeloupe). Bulletin De La Société Géologique De France. 2013;184:119–28. https://doi.org/10.2113/gssgfbull.184.1-2.119.

Reyes N, Vidal A, Ramirez E, Arnason K, Richter B, Steingrimsson B, Acosta O, Camacho J. Geothermal exploration at Irruputuncu and Olca volcanoes: pursuing a sustainable mining development in Chile. GRC Trans. 2011;35:983.

Rivera G, Cecioni M, Volpi G. Modelo Integrado 3D del Sistema Geotérmico "Cerro Pabellón" al Término de la Etapa de Construcción. Internal Report. (Internal Confidential Report). Geotérmica del Norte S.A. 2018.

Rivera G, Morata D, Ramirez C, Volpi G. Volcanic and tectonic evolution of Azufre – Inacaliri volcanic chain and Cerro Pabellón geothermal field (Northern Chile), in: proceeding of the World Geothermal Congress 2020+1. Reykjavik, Iceland; 2021.

Robinson D, Schmidt S, Santana de Zamora A. Reaction pathways and reaction progress for the smectite-to-chlorite transformation: evidence from hydrothermally altered metabasites. J Metamorph Geol. 2002;20(1):167–74. https://doi.org/10.1046/j.0263-4929.2001.00361.x.

Rowland J, Simmons F. Hydrologic, magmatic, and tectonic controls on hydrothermal flow, Taupo Volcanic Zone, New Zealand: implications for the formation of epithermal vein deposits. Econ Geol. 2012. https://doi.org/10.2113/econgeo.107.3.427.

Simmons SF, Browne PRL. Hydrothermal minerals and precious metals in the Broadlands-Ohaaki geothermal system: implications for understanding low-sulfidation epithermal environments. Econ Geol. 2000;95:971–99. https://doi.org/10.2113/gsecongeo.95.5.971.

Tassi F, Aguilera F, Darrah T, Vaselli O, Capaccioni B, Poreda RJ, Delgado Huertas A. Fluid geochemistry of hydrothermal systems in the Arica-Parinacota, Tarapacá and Antofagasta regions (northern Chile). J Volcanol Geoth Res. 2010;192:1–15. https://doi.org/10.1016/j.jvolgeores.2010.02.006.

Taussi M, Nisi B, Pizarro M, Morata D, Veloso EA, Volpi G, Vaselli O, Renzulli A. Sealing capacity of clay-cap units above the Cerro Pabellón hidden geothermal system (northern Chile) derived by soil CO2 flux and temperature measurements. J Volcanol Geoth Res. 2019;384:1–14. https://doi.org/10.1016/j.jvolgeores.2019.07.009.

Thomasson J, Kristmannsdottir H. High temperature alteration minerals and thermal brines, Reykjanes, Iceland. Contr Mineral Petrol. 1972;36:123–34. https://doi.org/10.1007/bf00371183.

Tibaldi A, Corazzato C, Rovida A. Miocene-Quaternary structural evolution of the Uyuni-Atacama region, Andes of Chile and Bolivia. Tectonophys Underst Stress Deform Active Volcanoes. 2009;471:114–35. https://doi.org/10.1016/j.tecto.2008.09.011.

Urzúa L, Powell T, Cumming WB, Dobson P. Apacheta, a new geothermal prospect in Northern Chile, in: Geothermal Resources Council Transactions. Davis, California: Geothermal Resources Council; 2002. p. 65–9.
Vásquez M, Bauluz B, Nieto F, Morata D. Illitization sequence controlled by temperature in volcanic geothermal systems: the Tinguiririca geothermal field, Andean Cordillera, Central Chile. Appl Clay Sci. 2016;134:221–34. https://doi.org/10.1016/j.clay.2016.04.011.
Veloso EE, Tardani D, Elizalde D, Godoy BE, Sánchez-Alfaro PA, Aron F, Reich M, Morata D. A review of the geodynamic constraints on the development and evolution of geothermal systems in the Central Andean Volcanic Zone (18–28°Lat.S). Int Geol Rev. 2019;62:1294–318. https://doi.org/10.1080/00206814.2019.1644678.
Vidal J, Genter A, Chopin F. Permeable fracture zones in the hard rocks of the geothermal reservoir at Rittershoffen, France. J Geophys Res Solid Earth. 2017. https://doi.org/10.1002/2017JB014331.
Vidal J, Patrier Mas P, Betancourt C, Maza S, Morata D. First results of the vein alteration in the deep well PGC1 of Irruputuncu geothermal system, Andean Cordillera, Northern Chile., in: World Geothermal Congress 2020+1. Reykjavik, Island; 2021.
Vidal J, Patrier P, Beaufort D, Maza S, Rivera G, Volpi G, Morata D. Clay minerals in the deep reservoir of the Cerro Pabellón geothermal system (Northern Chile). Minerals. 2022. https://doi.org/10.3390/min12101244.
Wojdyr M. Fityk: a general-purpose peak fitting program. J Appl Crystallogr. 2010;43:1126–8. https://doi.org/10.1107/S0021889810030499.

Publisher's Note